A GLOBAL OXIDATION SCHEME FOR PROPANE-AIR COMBUSTION SUITABLE FOR USE INTO COMPLEX REACTING FLOW COMPUTATIONS

P. K o u t m o s, G. G i a n n a k i s, P. M a r a z i o t i

Department of Mechanical and Aeronautical Engineering
University of Patras

Patras, Rio 26500, Greece

In Direct or Semi-Direct Numerical Simulations of turbulent reacting flows the exploitation of complex, realistic and detailed chemistry and transport models often results in prohibitive memory and CPU requirements when flows of practical relevance are treated.

The integrated Combustion Chemistry approach has recently been put forward as a methodology suitable for the integration of complex chemical kinetic and chemistry effects into large scale computational procedures for the calculation of complex and practical reacting flow configurations. Through this procedure, a reduced chemical kinetic scheme involving only a limited number of species and reactions is derived from a detailed chemical mechanism, so as to include major species and pollutants of interest in the main flow calculation. The chemical parameters employed in this integrated scheme i.e. rates, constants, exponents are then calibrated on the basis of a number of constraints and by comparing computations over a range of carefully selected laminar flames so as to match a number of prespecified flame properties such as adiabatic temperatures, selected target species profiles, flame speeds, extinction characteristics. The present work describes such an effort for a commonly used fuel of both the fundamental and practical importance that often is used to simulate the performance of higher hydrocarbons in practical engine simulations, i.e. propane. The proposed nine-step scheme involves nine major stable species and in addition to the basic propane oxidation model also includes NO_X production and soot formation submodels.

Key words: integrated Combustion Chemistry, reduced propane chemistry mechanisms, laminar flames, chemical reaction schemes.

NOTATIONS

A_k — preexponential factor in the Arrhenius law of reaction k,

A_s — particle surface area in soot model,

a — strain rate ($\sec^{-1}$) in counterflow flames,

C_v — constant in radiative flux expression,

c_p — specific heat,

C_a — constant in particle number density equation source term,

D, d — diameter,

$D_{i-\mathrm{N2}}$ — diffusion coefficient in binary mixture of the i-th species and nitrogen,

d_p — carbon particle diameter in soot model source term,

E_{NOx} — NOx emission index,

f_v — soot volume fraction,

H enthalpy,

H_i enthalpy of species i,

h_i absolute value of enthalpy,

h_{fi}^0 heat of formation at standard state,

I_{bik} Planck function in radiative flux expression,

I_f number of momentum equations solved,

k specific reaction rate constant,

Le_i Lewis number for species i,

M_s molecular weight of soot,

M_i molecular weight of species i,

N_s number of species,

N_A Avogadro number,

N_k number of species involved in reaction k,

P_s particle number density, in soot model,

P static pressure,

q_r radiative heat flux,

R_u universal gas constant,

R1...9   number of reaction in reduced scheme,

R_{cyl} radius in porous cylinder counterflow flame configuration,

r radial direction,

S_L laminar flame speed,

T temperature,

u axial velocity,

$u_{\mathrm{air},\infty}$ approach air velocity in porous cylinder counterflow flame configuration,

v radial velocity,

v_w fuel injection velocity in porous cylinder counterflow flame configuration,

X_i mole fraction of species i,

Y_i mass fraction of species i,

y y axis, transverse direction,

z z axis, axial direction,

w_i net rate of production of species i.

GREEK SYMBOLS

α_k temperature exponent in reaction step k,

Γ_Φ transport coefficients in governing equations,

ζ_{ik} intergration intensities in radiative flux expression,

$\eta_{c,\min}$ constant in particle number density equation source term,

λ thermal conductivity,

$\nu'_{i,k},\ \nu''_{i,k}$ stoichiometric coefficients in forward and backward direction,

$\nu_{i,k}$ concentration exponents of species i involved in reaction k,

π $3.14\ldots$,

ρ density,

σ_B Boltzmann constant,

$\Phi,\ \phi$ represents any variable (i.e. 1, u, v, H or Y_i) used in the governing equations,

$[\mathrm{CxHy}]$ molar concentration of species i.

b	backward,
ex	extinction,
f	forward,
s	soot,
k	reaction step,
i	species i,
Nucl	nucleation,
Growth	growth.

1. Introduction

The combustion of hydrocarbons for the production of energy is a common and important phenomenon in many engineering applications. In most practical devices, chemical reactions usually take place within and strongly interact with a turbulent flow, and the adequate description of the combustion process requires the consideration of a large number of fluid and chemical parameters [1]. On the other hand, during the past decade the demand for higher efficiencies, the stringent emission regulations and the need to reduce costs in design and optimization procedures for combustion chambers, has prompted the exploitation of Computational Fluid Dynamics methods in support of experimental procedures [2–4].

Direct or Semi-Direct Numerical Simulations (e.g. DNS, LES) of turbulent reacting flows offer a promising tool toward understanding of the complex physics of these flows. The full potential and advantages of these techniques can best be realized when sufficiently complex and realistic but flexible and tractable chemistry and transport models are exploited [2, 5]. Currently, computational costs and numerical considerations preclude spatially three-dimensional turbulent simulations with detailed chemistry and transport models in the parameter range of practical interest. Instead, the judiciously reduced chemical mechanisms that can be employed profitably within DNS or LES and provide a realistic description of appropriate thermochemical parameters are preferred [2, 3, 6].

A number of methodologies have been exploited to simplify a detailed mechanism e.g. the systematic consideration of steady-state and partial equilibrium assumptions leading to skeletal mechanisms [7], the analysis and categorization of characteristic chemical time-scales of separate reaction groups [8] and the Integrated Combustion Chemistry (ICC) approach [9], which involves the use of a limited number of judiciously chosen species and reactions with kinetic parameters tuned to match a prespecified number of constraints and flame properties. The ICC approach, alone or in conjunction with other methodologies, offers a viable alternative systematic reduction procedure, targeting specific require-

ments with reference both to the thermochemical submodels and to the complete computational procedure. In contrast to the first two approaches, [7, 8], it only involves a limited number of steps and focuses on major species and pollutants of interest for the main simulation, in the effort to avoid the burden of intermediate radicals and elementary rates altogether that would prohibitively burden the basic computational procedure.

The present work describes an effort along similar lines, to derive a simplified and tractable chemical scheme for the oxidation of propane, a fuel of practical interest, including NO_X and soot production models. Its chemical parameters are calibrated by using this scheme within one and two-dimensional reacting flow solvers and by computing a number of well documented one and two-dimensional and coflowing laminar flames, lifted and attached by matching a number of flame properties such as peak temperatures, major target species, flame speeds and extinction characteristics. The successful derivation and encouraging validation of the presently proposed scheme for propane lends support for an extension of the approach to more complex hydrocarbons, such as ethylene and alternative fuels of practical relevance such as H_2 and CH_3OH.

2. THE INTEGRATED COMBUSTION CHEMISTRY METHODOLOGY

2.1. The basic approach

The proposed approach is based on the requirement that the resulting mechanism must be able to predict, to a significant extent, what a state of the art multi-step reduced mechanism is predicting for one, two-dimensional and jet flames. The route to achieve this relies on the calibration of the rate parameters of a starting selected chemical scheme by computing laminar flames for which credible experimental data exist. In this investigation, the three-step reduced scheme given by KENNEL et al. [7] is chosen here as the starting mechanism for the basic methane oxidation:

$$C_3H_8 + 2O_2 \rightarrow 3CO + 3H_2 + H_2O, \tag{R1}$$

$$CO + H_2O \leftrightarrow CO_2 + H_2, \tag{R2}$$

$$2H_2 + O_2 \leftrightarrow 2H_2O. \tag{R3}$$

The original global rate parameters may be given in terms of linear combinations of many of the rates of the elementary reactions of the C_1-chain skeletal mechanism and may involve a number of intermediates and radicals (e.g. [7, 8, 10]). The original basic steps and species of (R1) to (R3) are retained but the target here is to produce global rates with simple kinetic parameters *exclud-*

ing altogether intermediate elementary rates and radicals in the resulting global rate expressions.

A framework to achieve this goal has been put forward by [9]. The *first* objective is prediction of the flame temperature and heat release in various cases. Because no extended product dissociation is allowed, the fuel heat of reaction is slightly (5%) reduced to reproduce the experimental temperatures. The *second* objective is the reproduction of variation of the laminar burning velocity versus mixture dilution as close as possible by regulating the pre-exponential constants (A_k), the activation energies (E_{Ak}) and the species exponents of the above three rates, to fit the available experimental data. An appropriate choice of a set of A_k, E_{Ak} and relevant exponents is additionally constrained by the adequate prediction of the extinction limits of selected opposed jet or stagnation point flames. The *third* objective is the adequate computation of targeted product species profiles for a range of strain rate values. This is interrelated with the requirement that the resulting scheme should be also capable of predicting unsteady effects, an aspect that represents the *fourth* objective and this is particularly significant in highly turbulent flame calculations and at conditions involving localized extinctions and reignitions. Here a strained counterflow flame configuration and a pulsating lifted-off coflow diffusion flame are used for such validation.

Apart from the choices for the chemistry model, the molecular transport model, can also affect the correct computation of the flame properties. As in massive complex flow simulations the simplified transport models are frequently exploited, (e.g. [2, 3, 6]), validation tests are here performed utilizing similar levels of complexity. Fick's law with constant Lewis numbers, Sunderland's law for viscocity, constant Prandtl and Schmidt numbers and temperature-dependent specific heats were presently employed. Only in the computations of the freely propagating 1-D premixed flames, diffusion coefficients in binary mixtures of the i-th species and N_2 were exploited.

Anticipating that radiative losses can have a significant influence on NO_X and soot levels, an optically thin radiation model was embodied in the calculations where it is assumed that the only significant radiating species are CO, CO_2, H_2O and soot. By employing an optically thin limit in which self-absorption of radiation is neglected, the divergence of the net radiative flux can be written as:

$$(2.1) \qquad \nabla q_r = C_V f_V T^5 + 4\pi \sum_{ik} \zeta_{ik} \rho_k I_{bik} ,$$

where f_v is the soot volume fraction and I_{bik} is the Planck function evaluated at the gas band centers of the contributing vibration-rotation or pure rotational bands, whose integrated intensities are given by ζ_{ik}. The value of the

constant C_V is here taken as $4.243 \cdot 10^{-10}$, with units that give a power density in watts/cc with T in Kelvins, according to the suggestions of references [6, 10].

2.2. *The proposed mechanism*

The basic oxidation of propane is here conveniently represented by the aforementioned three-step scheme of reaction set (R1) to (R3). Regarding the production of NO_X it has been established that the three main routes to NO formation are the prompt, the thermal and the N_2O mechanism [2, 9, 11], while in rich environments the reburn mechanism is also known to be important. The N_2O production path here is not directly accounted for; its contribution however is indirectly apportioned through the calibration of the rate constants in the employed NOx scheme on the basis of experimental data that include the N_2O levels. The proposed scheme takes into account the remaining contributions through the set of reactions:

$$0.5N_2 + [O] \leftrightarrow NO, \tag{R4}$$

$$0\,C_3H_8 + N_2 + O_2 + 0[O] + 0H_2O \leftrightarrow 2NO + 0C_3H_8 \,. \tag{R5}$$

The zero coefficients for C_3H_8, $[O]$ and H_2O in reaction (R5) mean that these species do not participate explicitly in this reaction but are included in the calibrated rate expressions. The required oxygen radical is here obtained from partial equilibrium assumptions [8, 11]. The involvement of water and oxygen radicals in the prompt production rate (e.g. Refs. [2, 11]) is therefore accounted for in the formulated reduced NOx reaction scheme. The influence of intermediates and radicals related to the fuel structure is necessarily mimicked through propane, which acts as a catalyst in reaction (R5).

To complete the overall scheme, a model for soot formation and oxidation has also been implemented employing many features from the successful soot model proposed by LINSTEDT [6, 10]. The underlying reactions for acetylene production are here all summed up and represented through one model reaction of the form:

$$2C_3H_8 \leftrightarrow 3C_2H_2 + 5H_2 \,. \tag{R6}$$

The corresponding soot nucleation and growth processes are addressed following the modeling assumptions of reference [10] and represented as:

$$C_2H_2 \rightarrow 2C_s + H_2 \,. \tag{R7}$$

The subsequent soot oxidation reactions due to OH radicals and O_2 is here modeled and expressed as:

$$C_s + 0.5O_2 \rightarrow CO, \tag{R8}$$

$$C_s + H_2O \rightarrow CO + H_2. \tag{R9}$$

In line with the integrated concept of the proposed mechanism, the radicals involved in the original mechanism (e.g. OH, H) have been replaced by stable species (e.g. H_2O, H_2) addressed in the proposed reduced scheme. The resulting soot chemical scheme is implemented and applied by solving two additional transport equations for particle number density and soot mass fraction, as discussed below in Sec. 3.

2.3. Determination of global mechanism kinetic rate parameters

The first step in the calibration procedure involves the identification of an appropriate set of A_k and E_{Ak} values for the hydrocarbon chemistry starting from the aforementioned basic oxidation scheme (reactions (R1) to (R3)). An iterative approach is then employed aiming to adjust the kinetic rate parameters A_k, E_{Ak} and determine any species exponents with respect to the four target requirements described in Sec. 2.1. With the simple transport formulations described previously, the kinetic parameters are tuned and adjusted through a series of repeated test computations involving the prediction of the temperature and species profiles, the flame speed and the extinction behavior of laminar one and two-dimensional and coflowing jet flames within the context of the discussions of Sec. 2.2 and the constraints of Sec. 2.1. With the propane oxidation scheme established, the NO_X reactions ((R4) and (R5)) are then added. The appropriate initial set of A_k and E_{Ak} values is here chosen with guidance from and reference to several features of the relevant elementary NO_X production steps, (e.g. Ref. [9]). These rate parameters are then similarly tuned in repeated test computations in which close prediction of the NOx levels in 1-D freely propagating and 2-D coflow jet flame configurations is required.

The rate parameters of reaction (R4) are calibrated to achieve the correct prediction of thermal NO_X levels and then the prompt (Fenimore) and reburn contributions are apportioned through reactions (R5) in the test cases described in Sec. 4. In an analogous fashion the soot reaction scheme is finally added and the rate constants for reactions (R6) to (R9) are adjusted to reproduce the correct levels of C_2H_2 and soot volume fraction for the test cases selected and discussed below. The final set of the kinetic rate parameters is given in Table 1.

Table 1. Specific reaction rate constants for reduced C_3H_8-air oxidation scheme.

Rxn No.	Preexponential (A_k)	Temperature exponent, (a_k)	Activation energy, (E_{Ak})	Species exponents
1	3.5E5	1	12500	$C_3H_8^{0.6}$, $O_2^{1.0}$
2,f	48750	1.65	-300	$CO^{0.8}$, $H_2O^{1.25}$
2,b	$1.825*10^6$	1.14	-1000	$CO_2^{0.8}$, $H_2^{1.15}$
3,f	$4.2*10^8$	-0.72	0	$H_2^{1.15}$, $O_2^{0.65}$
3,b	$1.25*10^8$	-0.7	0	$H_2O^{1.25}$
4,f	$1*10^{10}$	0.3	37770	$[O]^{0.97}$
4,b	$7*10^7$	0.9	20600	$NO^{0.745}$, $[O]^{1.04}$
5,f	$1.5*10^{10}$	0	11100	$C_3H_8^{0.03}$, $N_2^{1.16}$, $O_2^{0.03}$, $H_2O^{0.5}$, $[O]^{1.0}$
5,b	$8*10^8$	0	8100	$C_3H_8^{0.05}$, $NO^{1.56}$
6,f	$5*10^{21}$	-4.35	25198	$C_3H_8^{0.92}$
6,b	$7.5*10^{19}$	-3.8	34500	$C_2H_2^{0.95}$, $H_2^{0.01}$
7	As reported in [10]	As reported in [10]	23000	$C_2H_2^{0.01}$
8	As reported in [10]	0.4	23850	As reported in [10]
9	3.6	0.75	0	$C_S^{0.1}$, $H_2O^{1.7}$

Units in mole/cm^3, sec^{-1}, K, cal/mole (species exponents not declared above are unity).

3. THE NUMERICAL METHOD

The flame configurations studied here are simulated by solving the time-dependent form of the two-dimensional gas-phase conservation equations for reacting flow. The adopted methodology is similar to that of [12] and closely derives from the formulations of [4]. Conservation equations for mass, momentum, energy and species are solved and the equation set can be expressed in e.g. cylindrical coordinates (z, r) with the general form:

$$(3.1) \quad \frac{\partial (\rho\phi)}{\partial t} + \frac{\partial (\rho u\phi)}{\partial z} + \frac{\partial (\rho v\phi)}{\partial r}$$

$$= \frac{\partial}{\partial z}\left(\Gamma_\phi \frac{\partial \phi}{\partial z}\right) + \frac{\partial}{\partial r}\left(\Gamma_\phi \frac{\partial \phi}{\partial r}\right) - \frac{\rho v\phi}{r} + \frac{\Gamma_\phi}{r}\frac{\partial \phi}{\partial r} + S_\phi$$

ρ, u and v denote density, axial and radial velocities and, depending on the variable used for Φ (i.e. 1, u, v, H or Y_i), this general form represents the conservation of either mass, momentum, energy or species. The transport coefficients

Γ_Φ are obtained from the molecular transport model discussed previously while the source terms, S_Φ, are provided in Table 2, and their treatment is similar to that discussed in [12]. The enthalpy H is defined as:

$$H = \int_{T_0}^{T} c_p \, dt = \sum_{1}^{N_s} Y_i H_i = \sum_{1}^{N_s} Y_i (h_i - h_{fi}^0),$$

where h and h_f^0 represent the enthalpy and the heat of formation at standard state respectively.

Table 2. Transport coefficients and source terms appearing in governing equations.

Equations	ϕ	Γ_ϕ	S_ϕ
Continuity	1	0	0
Axial momentum	u	μ	$-\dfrac{\partial p}{\partial z} + (\rho_0 - \rho)g + \dfrac{\partial}{\partial z}\left(\mu\dfrac{\partial u}{\partial z}\right) + \dfrac{\partial}{\partial r}\left(\mu\dfrac{\partial v}{\partial z}\right) + \dfrac{\mu}{r}\dfrac{\partial v}{\partial z}$ $-\dfrac{2}{3}\dfrac{\partial}{\partial z}\left(\mu\dfrac{\partial u}{\partial z}\right) + \dfrac{\partial}{\partial z}\left(\mu\dfrac{\partial v}{\partial r}\right) + \dfrac{\partial}{\partial z}\left(\mu\dfrac{v}{r}\right)$
Radial momentum	v	μ	$-\dfrac{\partial p}{\partial r} + \dfrac{\partial}{\partial z}\left(\mu\dfrac{\partial u}{\partial r}\right) + \dfrac{\partial}{\partial r}\left(\mu\dfrac{\partial v}{\partial r}\right) + \dfrac{\mu}{r}\dfrac{\partial v}{\partial r} - 2\mu\dfrac{v}{r^2}$ $-\dfrac{2}{3}\dfrac{\partial}{\partial r}\left(\mu\dfrac{\partial u}{\partial z}\right) + \dfrac{\partial}{\partial r}\left(\mu\dfrac{\partial v}{\partial r}\right) + \dfrac{\partial}{\partial r}\left(\mu\dfrac{v}{r}\right)$
Species mass fractions	Y_i	ρD_{i-N_2}	$\dot{w}_i$
Energy	H	$\dfrac{\lambda}{c_p}$	$\nabla\left[\dfrac{\lambda}{c_p}\sum_{1}^{N_s}\left(\mathrm{Le}_i^{-1} - 1\right) H_i \nabla Y_i\right] - \sum_{1}^{N_s} h_{fi}^0 \dot{w}_i$

Le_i is the Lewis number of species i, defined as $\mathrm{Le}_i = \lambda/\rho c_p D_{i-N2}$, where D_{i-N2} is the diffusion coefficient of the i-th species in a binary mixture of that species and nitrogen. These binary diffusion coefficients were exploited only in the computations of the freely propagating 1-D premixed flame configurations. Also the global species and the state equations,

$$(3.2) \qquad Y_{N_2} = 1.0 - \sum_{1}^{Ns-1} Y_i, \qquad P = \rho R_u T \sum_{1}^{N_s} \dfrac{Y_i}{M_i}$$

where R_u is the universal gas constant, T is the temperature, M_i is the molecular weight of species i, together with the net rate of production of the i-th species

due to the number of chemical reactions N_k expressed as:

$$(3.3) \qquad w_{i,k} = \left(\nu''_{i,k} - \nu'_{i,k} \right) * A_k * T^{a_k} \exp \left\{ -\frac{E_{Ak}}{R_u T} \right\} \prod_{i=1}^{N_k} \left(\frac{\rho Y_i}{M_i} \right)^{\nu_{i,k}}$$

which appear in the source terms of the species conservation equations, complete the set of governing equations. Here Y_i is the mass fraction of the species i, $\nu'_{i,k}$ and $\nu''_{i,k}$ are the stoichiometric coefficients of species i in reaction k in forward and backward direction, $\nu_{i,k}$ are concentration exponents of species i involved in reaction step k, A_k and E_{Ak} are the preexponential factor and activation energy in the Arrhenius law of reaction k.

The computational domain in each different test case is commonly bounded by inflow and outflow boundaries, wall and symmetry or axis planes. Constant values of the variables were specified at inlet sections, with velocity, temperature and mixture compositions taken from the reported experiments. At lines of symmetry the radial (normal) velocity was set to zero and a zero gradient was assumed for the axial velocity, temperature and species concentrations. A zero gradient was applied at the outflow boundaries that were carefully located far away from regions of steep gradients of the variables. Open boundaries were implemented as slip lines where a zero radial (normal) velocity and a zero gradient condition for axial velocity, temperature and species concentrations were applied. The governing equations are integrated by using a finite-volume approach with a staggered, non-uniform grid system. The momentum equations are discretized using an implicit QUICKEST finite-difference scheme (KOUTMOS *et al.* [4]), while a hybrid scheme is employed for stability in the species equations. An iterative alternating direction implicit (ADI) technique [12] is used for solving the set of $N_s + I_f + 1$ algebraic equations ($N_s + 1$ is the number of species and the enthalpy equation and I_f represents the number of the momentum equations solved, depending on the dimensions of the configuration studied). A stable numerical integration procedure is achieved by coupling the species and energy equations through the chemical reaction source terms and the chemical source terms are linearized to improve convergence. The pressure field is calculated at every time step by solving the pressure Poisson equations in every grid node simultaneously and exploiting the LU (Lower and Upper diagonal) matrix decomposition technique. For the validation test runs involving freely propagating premixed flame configurations, the standard PREMIX Sandia code [13] was used. The extinction behavior of non-premixed stagnation point flames to steady and unsteady strain rate were investigated by adapting the basic two-dimensional detailed flow solver to the particular flame/geometry configuration.

The chemical reaction scheme for soot production and oxidation is combined with the solution of two additional model transport equations for particle number density, P_s, and soot mass fraction, Y_s, as proposed by [6]. These have the same

form as Eq. (3.1), written for the i-th species as given in Table 2. Chemical reaction (R7) represents here both nucleation and growth while reactions (R8) and (R9) represent the soot oxidation process.

The relevant source term, S_{Ys}, for soot mass fraction, Y_s, can then be written:

$$(3.4) \quad S_{Y_s} = 2k_{7,\text{Nucl}} \left[C_2H_2 \right] M_s$$

$$+ 2k_{7,\text{Growth}} A_s \left[C_2H_2 \right] M_s - k_8 A_s \left[O_2 \right] M_s - k_9 A_s \left[H_2O \right] M_s$$

while that for particle number density, P_s, can be expressed as:

$$(3.5) \quad S_{P_s} = 2k_{7,\text{Nucl}} \left[C_2H_2 \right] \frac{N_A}{\eta_{C,\text{min}}} - 2C_a d_p^{1/2} \left(\frac{6\sigma_B T}{\rho_s} \right) (\rho P_S)^2 .$$

According to the recommendations of references [6, 10] the following set of constants is utilized in the above source expressions. M_s and ρ_s are the molecular weight and density of soot, $\sigma_B = 1.38 \cdot 10^{-23}$ J/K is the Boltzmann constant, $N_A = 6.022 \cdot 10^{26}$ particles/kmol is the Avogadro number, $C_a = 9$, $\eta_{c,\text{min}} = 60$ and $A_s = \pi d_p^2 \rho \, P_s$ is the particle surface area with $d_p = (6Y_s/\pi\rho_s P_s)$, the carbon particle diameter. Here the nucleation and growth rate constants used above, $k_{7,\text{Nucl}}$ and $k_{7,\text{Growth}}$ for reaction (R7), and the oxidation rate constant due to oxygen, k_8, are taken as suggested by [6, 10] with only minor changes as indicated in Table 1, while the rate constant, k_9, due to soot oxidation from OH is duly modified to take into account the replacement of the radical OH contribution in reaction R9 with the stable available species H_2O. The tuned reaction rate constants for reactions (R6) to (R9) are also given in Table 1.

4. RESULTS AND DISCUSSION

The performance of the basic oxidation mechanism was evaluated by computing unstretched laminar premixed propane-air flames having different equivalence ratios, Φ. An important validation parameter is the laminar flame speed, S_L, which was presently calculated and is compared against experimental data from the extended literature (e.g. references [2, 6, 7]) as a function of equivalence ratio Φ in Fig. 1a. The predicted lean and stoichiometric part of the S_L curve appears quite satisfactory with a peak S_L of 0.45 m/sec against experimental values in the region 0.39 to 0.47. The rich S_L branch however seems to be underpredicted possibly due to exclusion of intermediate radicals such as H and OH. In an initial effort to alleviate, in a simple manner, this rich branch deficiency and allow a more fruitful exploitation of the proposed scheme, a parameterization and tabulation of the preexponential factor of reaction (R3) as a simple function of the local equivalence ratio was attempted targeting the more correct prediction of the rich S_L branch values as depicted in Fig. 1a. A more
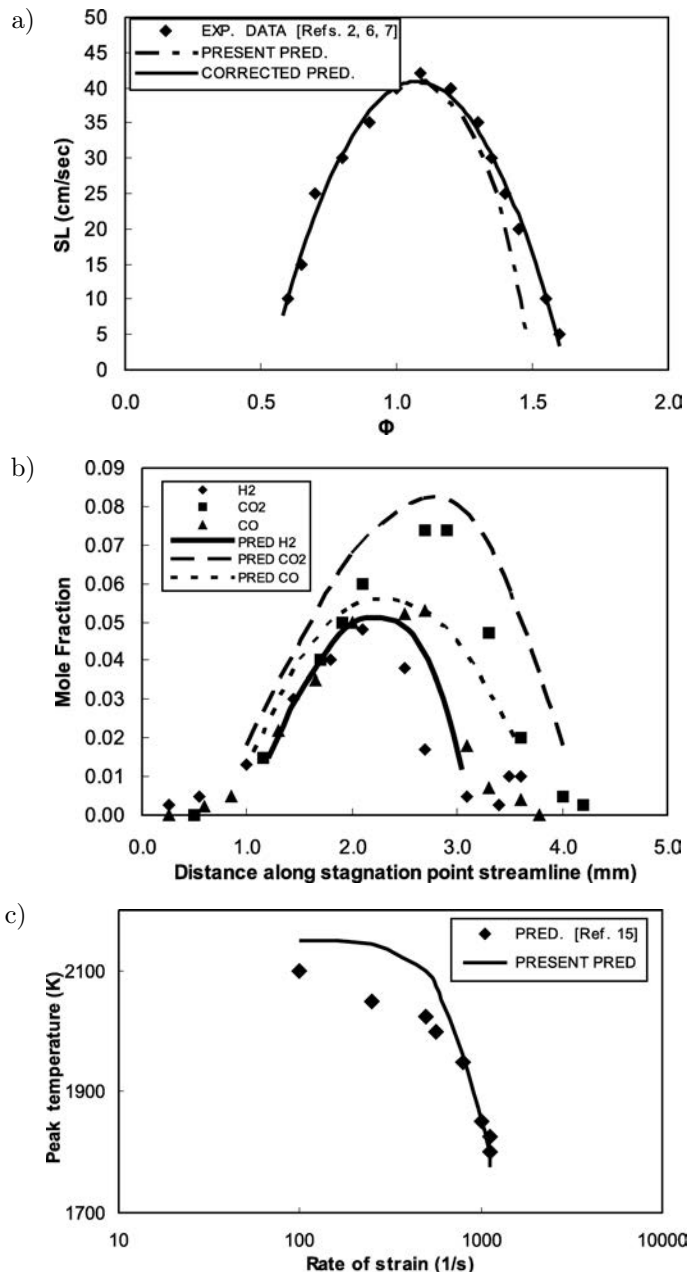
FIG. 1. a) Comparison between computed with the present reduced scheme (- - - -, —) and experimental (◆), Refs. [2, 6], laminar flame speeds over a range of equivalence ratios for freely propagating premixed flames; b) Comparisons between present calculations (lines) and measurements of [14] (points) in a counterflow diffusion flame configuration for major species profiles; c) Peak flame temperature as a function of the strain rate in the stagnation point diffusion flame of Ref. [14]. Computations from Ref. [15] with a four-step reduced mechanism (◆), present computations (—).

elaborate and extended approach along these lines can be applied by following the approach of reference [5] when more involved chemical schemes are adapted to local conditions and constraints.

The reduced scheme (R1) to (R3) was subsequently tested by computing a stagnation point diffusion flame in front of a porous cylinder (Tsuji-type burner, Fig. 3b, [14]) in a one-dimensional calculation by reformulating the detailed mathematical model of Sec. 3. Computed major species and temperature profiles for a strain rate, $a = u_{air,\infty}/R_{cyl}$, of 150 sec^{-1} and a fuel injection velocity v_w of 0.112 m/s (see Fig. 3b), agreed well with the classical experimental results of TSUJI and YAMAOKA [14] as shown in Fig. 1b. The computed unstretched flame peak temperature lies around 1950 K below the adiabatic value due to effects of transport processes and finite reaction rates. The presently calculated drop in the peak temperature with increasing strain rate (a) is adequately supported in similar calculations by JONES and LINDSTEDT [15] as displayed in Fig. 1c. As the strain rate, a, increases the peak temperature drops due to reactant leakage until no steady state solution exists and this point corresponds to the extinction limit. The computed a_{ex} is 645 sec^{-1} while the measurements of reference [14] suggested a value of about 670 sec^{-1}.

Amongst the various flame configurations used for the present scheme calibration, the one selected for discussion here is from the range of opposed jet burner (Fig. 3c) flame studies reported by WEHRMEYER et al. [16]. Specifically the structure of partially premixed opposed jet C_3H_8-air flames produced by counterflowing reactant jets of disparate and very lean or very rich stoichiometry i.e. a lean H_2-air jet impinging on a rich or lean C_3H_8-air jet, was experimentally and computationally investigated in that work (Fig. 3c). The resulting complex type of flames are of relevance to combustion processes occurring under stratified charge mode operation of direct injection spark ignition engines, where a flame in a region of burnable stoichiometry supports combustion in adjacent lean or rich regions that are outside the ignitable limits and thus represent a stringent test of the presented reduced scheme.

Here one partially premixed flame of a C_3H_8-air jet ($\Phi = 1.25$) opposing a H_2-air jet ($\Phi = 0.4$) at a strain rate of 180 s^{-1} was chosen for computation as it represents a stringent test for the proposed model. The results of the comparisons between the present numerical calculations and the measurements and computations, obtained by WEHRMEYER et al. [16], with the extended C_3H_8-air mechanism M5 as reported in Reference [2], are shown in Figs. 2a and 2b. The present computations are in good agreement with the reported temperature and species profiles except for their narrower width due to a slower rise of temperature and species on the rich fuel side. This is due to a weaker penetration of the triple flame into the rich fuel side. This is not unexpected since the uncorrected calibrated reduced sheme produces a lower flame propagation rate, S_L, when

we move toward the rich equivalence ratios, as discussed previously with respect to the underprediction of the experimental S_L branch in Fig. 1a. The calibrated mechanism, when corrected by employing a local adjustment of the (R3) reaction rate preexponential factor as a function of the prevailing local equivalence ratio, results in an improved agreement in the predicted temperature profiles as illustrated in Fig. 2a. The adjusted calculations, due to the locally increased reaction rates, exhibit an extended reaction zone profile that now reaches deeper toward the premixed fuel supply, as indicated by the comparisons shown in Fig. 2a, with consequent improvements in the species profiles as well (lines without correction are not shown for clarity in Fig. 2b).
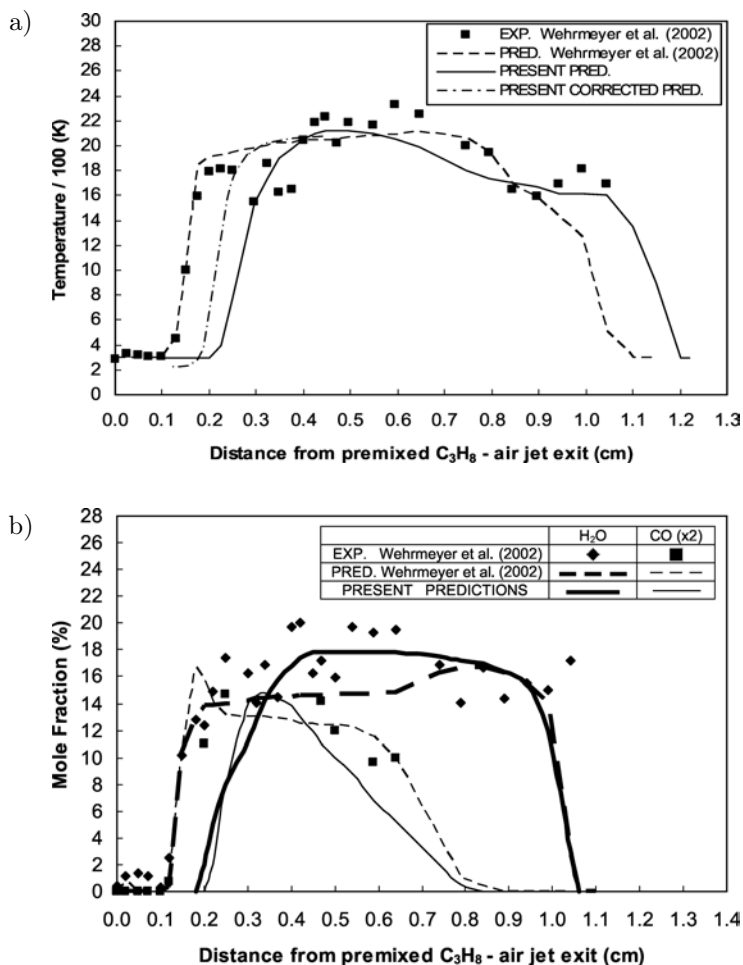
FIG. 2. Comparisons between present calculations (lines) and measurements and computations of WEHRMEYER et al. (symbols, dashed line) in an opposed jet burner premixed flame configuration: a) for the mean temperature profile along the burner stagnation axis; b) for the mean CO and H_2O profiles along the burner stagnation axis.

   Subsequently a range of two-dimensional axisymmetric coflowing laminar jet diffusion flames, with or without partial premixing, attached and lifted were calculated targeting at the qualitative and quantitative reproduction of major species, temperature, NO_X and soot production. Any discrepancies identified in these test runs led to readjustment of the reduced chemical scheme rate para-meters that were fed back to the runs for the one-dimensional flames discussed above; this iterative cycle produced the final tuned set of the chemical rate pa-rameters of Table 1.
   A sketch of the two-dimensional axisymmetric geometry burner configuration employed in the two-dimensional computations is given in Fig. 3a. It includes a fuel supply, an oxidizer supply and in certain test cases – a coflowing surrounding air stream. In the first test case the range of coflowing diffusion flames studied by WON et al. [17] were computed. Fuel (a mixture of C_3H_8/N_2 at 0.1486/0.8514 by mass) and air, both coflowed at various velocity ratios and formed a rich va-riety of diffusion flames ranging from attached, slightly detached, lifted and also oscillating from the burner rim. Temperature contours predicted by the present two-dimensional formulation employing the above proposed reduced scheme are shown in Figs. 4a, b and c depicting three fuel velocity conditions with none, moderate and significant lift-off from the burner exit. The characteristic fishbone structure at the base as well as the high temperature regions and the overall flame shape have been captured well when compared with the flow visualization photographs reported by WON et al. [17].


[FIG. 3a]

b)

c)
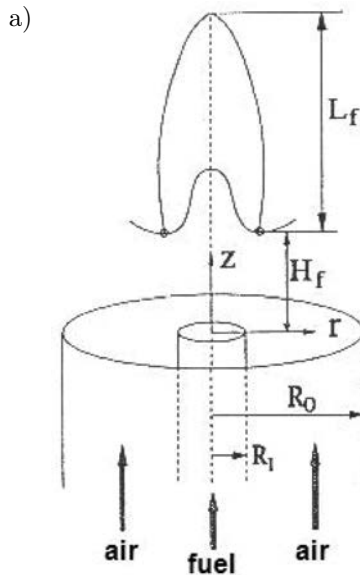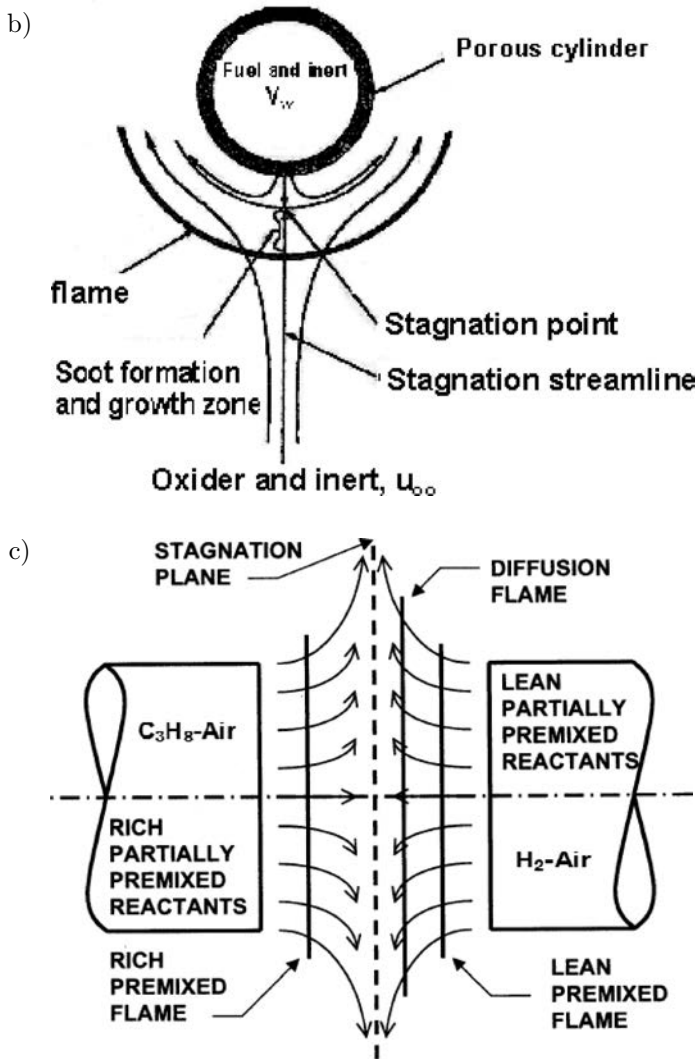
FIG. 3. a) Unconfined coflowing axisymmetric laminar diffusion flame burner configuration used in the computations; b) Porous cylinder counterflow diffusion flame configuration used in the computations (Refs. [14, 20, 21]); c) Opposed jet burner configuration used in the computations (Ref. [16]).

In the experiments of WON *et al.* [17] it was also found that as fuel velocity increases, in the intermediate velocity range, a regime can be identified, where the lift-off height varies intermittently between distinct lower and higher values, a feature that reportedly has been related to propane lift-off behaviour in other investigations as well [17]. As unsteady effects play an important role during localized extinctions and reignitions in highly turbulent flames, it was thought of interest to address the whole extent of the variation of the flame lift-off height
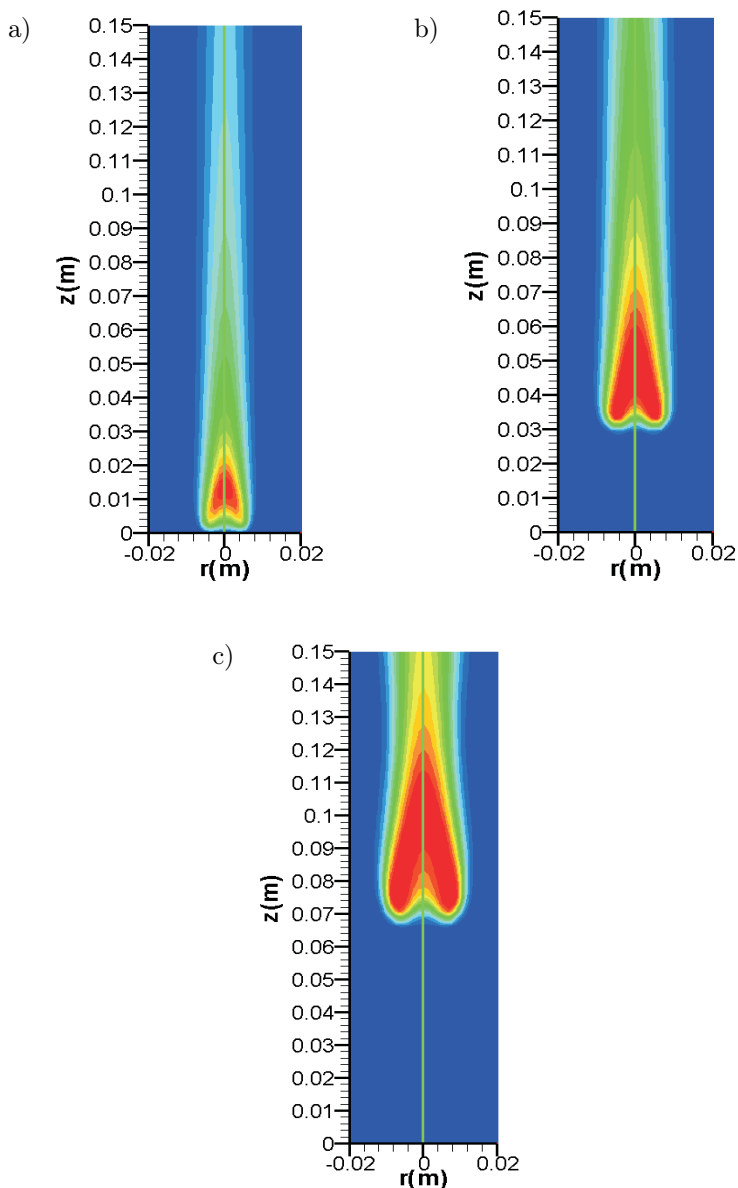
FIG. 4. Computations of temperature isotherm topology for the axisymmetric coflowing jet burner configuration studied by WON *et al.* [17]: a) attached flame, b) moderately lifted flame, c) highly lifted flame.

with fuel velocity change for the flames studied by WON *et al.* [17] to establish the capability of the method to predict inherent unsteady flame behaviour. Figure 5 displays the calculated variation of lift-off height along with the experimentally reported values. Both the attached and lifted flame lengths and lift-off

heights have been reproduced quite satisfactorily while, quite encouragingly, the oscillating flame regime, as indicated by the two branches in the graph, has also been retrieved by the present model. Evidently the presently proposed scheme produces an adequate response to the unsteady strain field produced by the pulsating nature of the flames, despite some quantitative differences in the reported values for the upper lift-off heights.
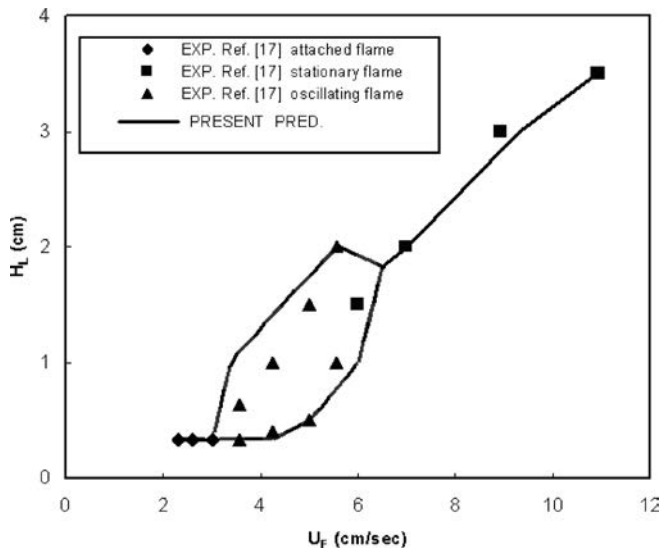

FIG. 5. Comparisons between predicted with the present scheme (line) and experimentally established in WON et al. [17] (symbols) of the variation of the flame lift-off height with fuel exit velocity (note the pulsating flame behaviour indicated by the displayed loop).

Subsequently, the capability of the proposed NOx module to capture the NOx production levels was tested. HEWSON [18] has reported a series of bulk NOx emissions measurements in laminar coflow, nonpremixed jet flames for a wide range of exit propane velocities and burner diameters while retaining the constant air coflow velocity. The reported emission index is expressed as $E_{NOx} = (3X_{NOx}M_{NO2}1000)/(X_{CO2}M_{Fuel})$, where X_i and M_i are the mole fraction and the molecular weight of species i, and this expression includes both the NO and NO_2 contributions. A comparison of the emissions calculated by the presently tuned scheme (the basic oxidation model now including reactions (R4) and (R5)) against a sample from the reported variations is displayed in Fig. 6. Despite the fact that the NO_2 contribution is not accounted for in the present model explicitly but only through tuning and calibration of the constants involved in the prompt rate expressions, the experimental trend and levels are reproduced encouragingly well. As a further test, the NOx levels (including thermal, prompt and N_2O contributions) reported in the work of BOCKHORN et al. [11]
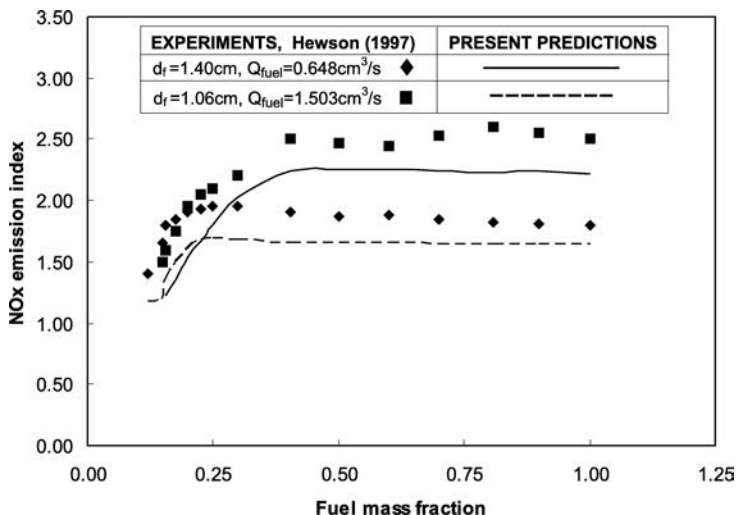
FIG. 6. Comparisons between presently predicted (lines) and experimental (HEWSON [18], symbols) variations of the emission index E_{NOx} with fuel dilution at two fuel velocities in the axisymmetric coflowing burner configuration.

for a range of lean partially premixed 1-D propane flames were additionally studied to further tune the present NOx model. Following the experimental conditions, calculations were run for an inlet mixture temperature of 400°C and a range of equivalence ratios corresponding to an adiabatic flame temperature variation from 1290°C to 1540°C. Results from the present computations are compared, in Fig. 7, with experimental and calculated results reported by
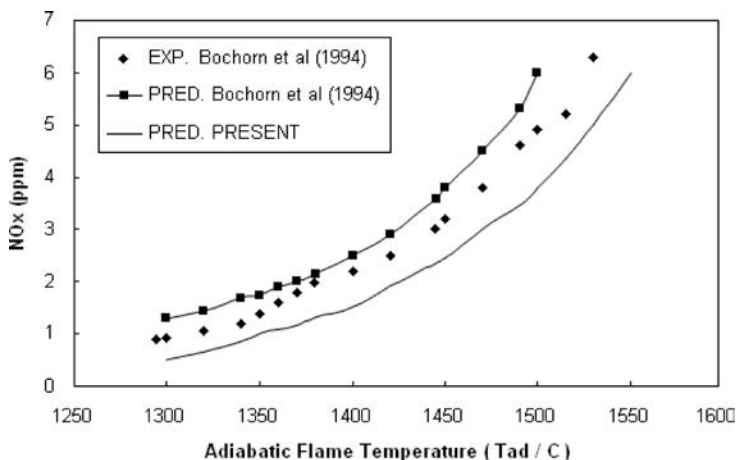

FIG. 7. Comparisons between present predictions (—) and experimental (♦) and computational (–♦–) results from BOCKHORN et al. [11], of the distribution of the NOx concentration levels in a flat premixed 1-D flame burner configuration with variation in the mixture equivalence ratio.

BOCKHORN *et al.* [11], who employed a version of the GRI 3.0 mechanism (e.g. Ref. [19]). Both the trend and the level of variation of the experimental results with mixture strength are apparently reproduced quite adequately by the tuned ((R4) and (R5) reactions) scheme.

The soot model was finally added to the basic C_3H_8 oxidation mechanism, tuned, calibrated and tested in a range of flame configurations. As an example, calculations for two C_3H_8 sooting counterflow diffusion flame arrangements (Fig. 3b), studied by VANDSBURGER *et al.* [20] and LAW *et al.* [21] are here discussed. Additional transport equations with source terms given by Eqs. (3.3) and (3.5) and the reactions (R6) to (R9) were now employed in these computations. The present model predicts the general shape, structure and peak temperature levels of this complex flame configurations. The level of agreement for the major species was of similar good quality as that encountered in the previously discussed computations. Within the context of the present reduced scheme, a critical factor in reproducing the measured soot distributions is the adequate reproduction of the acetylene profile concentrations, the only soot precursor addressed in the reduced scheme, since benzene is here excluded. Levels of C_2H_2 were computed with maximum discrepancies in peak values of less than 12% (e.g. compared with the measured peak values given in reference [20]). The effect of oxygen enrichment in the counterflow flames of VANDSBURGER *et al.* [20] and the predicted trends in soot production for two levels of fuel enrichment are subsequently shown in Fig. 8. Calculated peak soot volume fractions are in good agreement with experimental values while the variation along the centerline is

| Fuel dilution	PRESENT PRED.	Vandsburger et al (1988)
24%	———	◆
28%	- - - - -	■
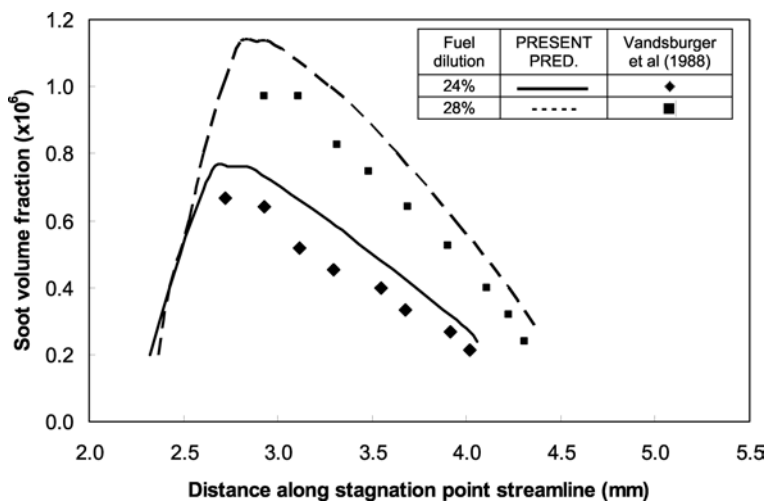
FIG. 8. Comparisons between present predictions with the proposed reduced scheme (lines) and experimental and measured by VANDSBURGER *et al.* [20] (symbols) soot volume fractions for counterflowing C_3H_8-O_2-N_2 flames with varying levels of O_2 enrichment.

captured well. Peak temperatures and major species addressed by the proposed mechanism were also in good agreement with the reported measurements. Next the influence of inert additives and/or air enrichment (25% O_2) in sooting counterflow flames measured by LAW et al. [21] was studied with the above proposed mechanism. Figure 9a displays the measured and presently computed variation of the temperature along the distance from the burner surface for a fuel mixture of $20\%He$–$80\%C_3H_8$ in this counterflow configuration. The good agreement
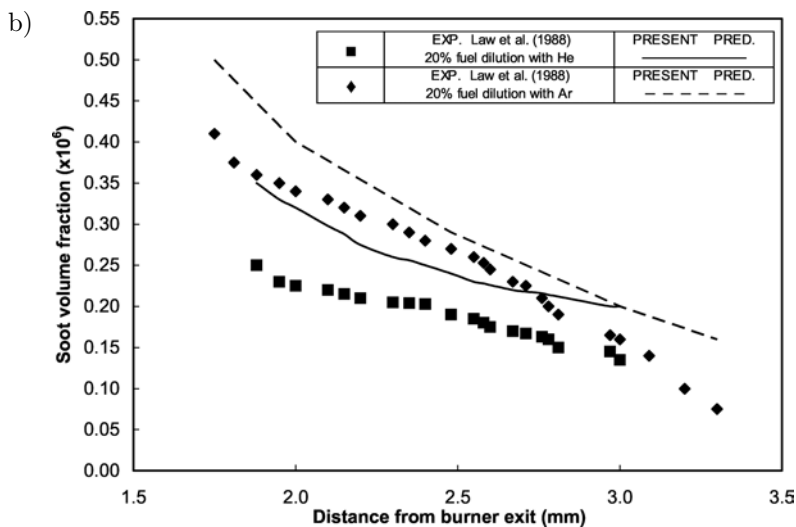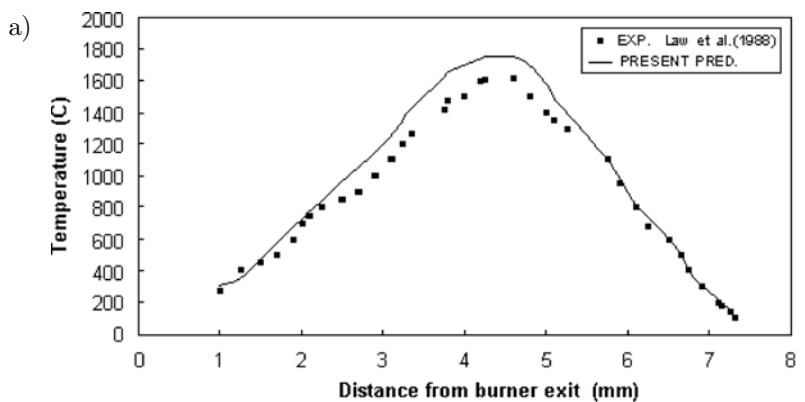

FIG. 9. a) Comparisons between present predictions with the proposed reduced scheme (lines) and experimental and measured by LAW et al. [21] temperature distributions with distance from burner exit for propane-air counterflowing diffusion flame with inert addition on the fuel side $2(0\%He$–$80\%C_3H_8)$. b) Comparisons between present predictions with the proposed reduced scheme (lines) and measurements by LAW et al. [21] of soot volume fraction distributions as a function of distance from burner surface for propane-enriched air (25%) counterflowing diffusion flame with different inerts added on the fuel side.

between measurements and predictions allows a meaningful evaluation of the soot model. Figure 9b displays predictions and experimental data for soot volume fraction at 20% fuel dilution by two different inert additives, namely He and Ar and air enrichment with oxygen maintained at 25%. Although some quantitative discrepancies are evident, it is most encouraging to see that the measured trends are reproduced quite well. This lends some credibility in the models sensitivity to delineate between different soot loadings due to different flame conditions.

From the above described test runs and comparisons it appears that the proposed reduced scheme has an acceptable and consistent behavior over the range of flame conditions investigated, and adequately predicts the target characteristics of Sec. 2.1 for the diffusion and premixed flame configurations studied. Inaccuracies apparently increase locally for rich mixtures beyond an equivalence ratio of about 1.3 e.g. in the test runs for the lifted flame. This aspect might be conveniently remedied to a large extent by employing concepts of adaptive chemistry as in Reference [5] and locally adjusting (at each computational grid node and time-step) selected parameters of the reduced scheme in accordance with the prevailing local flame conditions. Here, following a less involved approach along these lines proved the promising gains that may accrue from such a more general procedure; the flame speed was augmented for rich compositions (i.e. when the mixture strength locally exceeded 1.3) through an appropriate parameterization and tabulation of the preexponential factor of reaction (R3) as a simple function of the local equivalence ratio, thus improving the performance of the chemical scheme over an extented range of mixture compositions.

5. SUMMARY AND CONCLUSIONS

An Integrated Combustion Chemistry approach has been employed to derive a reduced oxidation scheme for a technically significant fuel, propane, including submodels for NOx and soot production. The complete scheme involves nine reactions and nine species focusing on major and stable species and pollutants, while avoiding altogether the computational burden of intermediate radicals and elementary rates. The chemical rate parameters were calibrated by systematically computing a range of well-documented one-dimensional freely propagating, premixed and stagnation point diffusion flames as well as two-dimensional axisymmetric coflowing jet diffusion flames, lifted and attached. Its overall performance has been encouraging and with further tests and refinements it can be valuable in large-scale computations of complex turbulent reacting flows. The procedure can be systematically extended to other practical fuels such as higher hydrocarbons, ethylene or alternative fuels of technological interest such as hydrogen, methanol and ethanol.

Acknowledgments

References

1. P. A. Libby and F. A. Williams, *Turbulent reacting flows*, Abacus Press, New York 1993.

2. D. Haworth, B. Cuenot, T. Poinsot and R. Blint, *Numerical simulation of turbulent propane-air combustion with non-homogeneous reactants*, Combustion and Flame, **121**, 395–422, 2000.

3. W. K. Bushe and R. W. Bilger, *Direct numerical simulation of turbulent non-premixed combustion with realistic chemistry*, Annual Research Briefs, Center for Turbulence Research, NASA Ames/Stanford University, 3–22, 1998.

4. P. Koutmos, C. Mavridis and D. Papailiou, *A study of turbulent diffusion flames formed by planar fuel injection into the wake formation region of a slender square cylinder*, Proc. Combust. Inst., **26**, 161–168, 1996.

5. W. H. Green and D. A. Schwer, *Adaptive chemistry*, Computational Fluid and Solid Mechanics, **32**, 1209–1211, 2001.

6. K. M. Leung, P. R. Lindstedt and W. P. Jones, *A simplified reaction mechanism for soot formation in nonpremixed flames*, Combust. and Flame, **87**, 289–305, 1991.

7. C. Kennel, J. Gottgens and N. Peters, *The basic structure of lean C_3H_8 flames*, Proc. Comb. Inst., **23**, 479–485, 1990.

8. U. Mass and S. B. Pope, *Simplifying chemical kinetics: Intrinsic low-dimensional manifolds in composition space*, Combustion and Flame, **88**, 239–264, 1992.

9. B. Bedat, F. N Egolfopoulos and T. Poinsot, *Direct numerical simulations of heat release and NO_X formation in turbulent non-premixed flames*, Combustion and Flame, **119**, 69–83, 1999.

10. P. R. Lindstedt, *Simplified soot nucleation and surface growth steps for non-premixed flames*, [in:] *Soot Formation in Combustion*, H. Bockhorn [Ed.], pp. 417–429, Springer Verlag, Heidelberg 1994.

11. H. Bockhorn, F. Mauss, A. Schlegel, S. Buser, and P. Benz, *NOx formation in lean premixed noncatalytic and catalytically stabilized combustion of propane*, Proc. Combust. Inst., **25**, 1019–1026, 1994.

12. V. R. Katta, L. P. Goss and W. M. Roquemore, *Effect of nonunity Lewis number and finite-rate chemistry on the dynamics of a hydrogen-air jet diffusion flame*, Combustion and Flame, **96**, 60–74, 1994.

13. R. J. Kee, J. F. Grcar, M. D. Smooke and J. A. Miller, *A Fortran program for modeling steady laminar one-dimensional premixed flames*, Sandia National Laboratories, Livenmore, C.A., 1985.

14. H. Tsuji and I. Yamaoka, *Structure analysis of counterflow diffusion flames in the forward stagnation region of a porous cylinder*, Proc. Combust. Inst., **13**, 723–730, 1971.

15. W. P. JONES and P. R. LINDSTEDT, *The calculation of the structure of laminar counter-flow diffusion flames using a global reaction mechanism*, Combust. and Flame, **61**, 31–49, 1988.

16. J. A. WEHRMEYER, Z. CHENG, D. M. MOSBACHER, R. W. PITZ, and R. OSBORNE, *Opposed jet flames of lean or rich premixed propane-air reactants versus hot products*, Combust. and Flame, **128**, 232–241, 2002.

17. S. H. WON, S. H. CHUNG, M. S. CHA, and B. J. LEE, *Lifted flame stabilization in developing and developed regions of coflow jets for highly diluted propane*, Proc. Combust. Inst., **28**, 2093–2099, 2000.

18. J. C. HEWSON, *Pollutant emissions from nonpremixed hydrocarbon flames*, PhD. Thesis, University of California, San Diego 1997.

19. G. P. SMITH, D. M. GOLDEN, M. FRENKLACH, N. W. MORIARTY, B. EITENER *et al.*, GRI-Mech version 3.0, http://www.me.berkeley.edu/gri-mech/

20. U. VANDSBURGER, I. KENNEDY, and I. GLASSMAN, *Soot formation in oxygen enriched counterflow diffusion flames of C_2H_4 and C_3H_8*, Combust. Sci. and Technol., **39**, 263–285, 1984.

21. C. K. LAW, R. L. AXELBAUM, and W. L. FLOWER, *Preferential diffusion and concentration modification in sooting counterflow diffusion flames*, Proc. Combust. Inst., **22**, 379–386, 1988.